Please cite this article in press as: Demirbas et al., G12 mutations rewire allosteric communication at the Ras–RalGDS interface, Biophysical Journal (2026), https://doi.org/10.1016/j.bpj.2026.01.053

Biophysical Journal
Article

Biophysical Society

G12 mutations rewire allosteric communication at the Ras–RalGDS interface

Emir Demirbas,[1] Hyunbum Jang,[2] Kayra Kosoglu,[3] Ruth Nussinov,[2,4,*] Attila Gursoy,[5,*] and Ozlem Keskin[1,*]
[1]Department of Chemical and Biological Engineering, Koc University, Istanbul, Turkey; [2]Computational Structural Biology Section, Frederick National Laboratory for Cancer Research in the Cancer Innovation Laboratory, National Cancer Institute, Frederick, Maryland; [3]Department of Molecular Biology and Genetics, Koc University, Istanbul, Turkey; [4]Department of Human Molecular Genetics and Biochemistry, Sackler School of Medicine, Tel Aviv University, Tel Aviv, Israel; and [5]Department of Computer Engineering, Koc University, Istanbul, Turkey

ABSTRACT The Ras subfamily is the most extensively studied branch of the Ras superfamily, with 20% of all human tumors having activating mutations in one of the *RAS* genes. Recent studies have shown that the Ras/RalGDS/Ral pathway plays a more significant role in the progression of Ras-driven colon and pancreatic cancers than the Ras/Raf and Ras/PI3K pathways. In this study, we investigated the interaction between Ras and the Ras/Rap binding domain (RBD) of RalGDS using long-time-scale molecular dynamics simulations. The binding free energy of dimerization showed that Rap1–RBD has the strongest interaction and M-Ras–RBD the weakest interaction among the simulated systems, consistent with experimental results. We noticed that Ras uses the same acidic interface residues when binding to the complementary basic residues of RalGDS and Raf. By analyzing bonding profiles, we identified several conserved interactions across different systems as well as isoform- and mutant-specific preferences. Our results demonstrate that G12D/V mutations favor Glu37-mediated stabilization, specifically through the $Glu37^{Ras}$–$Ser817^{RBD}$ hydrogen bond and the $Glu37^{Ras}$–$Tyr815^{RBD}$ anion-π interaction. By mapping interface allosteric communication pathways, we illustrated the interplay between these stabilizing interactions and allosteric signal transduction across the dimer. We hypothesize that communication between the Ras active site and the RalGDS RBD is rewired upon G12 mutations. Specifically, we identified the GTP–Gly/Asp/$Val12^{Ras}$–$Gln61^{Ras}$–$Tyr64^{Ras}$–$Ile36^{Ras}$–$Ile803^{RBD}$ pathway that exhibits divergent behavior in wild-type versus mutant systems. The interaction dynamics represented here may serve as a good reference point for studies aiming to develop mutant-specific targeting against tumors harboring Ral overactivity.

SIGNIFICANCE Ras GTPases are critical hub proteins that serve as binary switches in various signaling pathways involved in cell growth, proliferation, and differentiation. The Ras/RalGDS/Ral signaling pathway plays a crucial role in the development of colon and pancreatic cancers. Here, we employed all-atom molecular dynamics (MD) simulations to uncover the atomistic details of the interaction between Ras family members (K-Ras4B, H-Ras, M-Ras, and Rap1) and RalGDS Ras/Rap binding domain (RBD). Additionally, we simulated G12D/V mutants of K-Ras4B and H-Ras to investigate how these mutations impact the interaction mechanism. Our results provide a comprehensive mechanistic explanation of how the interactions differ across different Ras isoforms and mutants. As our study is the first comprehensive MD investigation of Ras–RalGDS RBD interaction, it can serve as a starting point for targeting studies.

INTRODUCTION

In eukaryotic cells, small guanosine triphosphatase (GTPase) proteins participate in a wide range of cellular processes, such as cellular growth, gene expression, membrane trafficking, differentiation, and cytoskeletal organization, in response to various extracellular stimuli (1). With more than 50 effectors, Ras GTPases constitute the most widely investigated members of the small GTPase family (2–5). They function as binary molecular switches in different signal transduction pathways by cycling between the guanosine diphosphate (GDP)-bound inactive form and the GTP-bound active form (6). Two flexible regions, called switch I and switch II, comprise the effector lobe and are responsible for the conformational changes induced by GDP-GTP exchange (7). Prior to effector binding, switch

Submitted November 21, 2025, and accepted for publication January 29, 2026.

*Correspondence: nussinor@mail.nih.gov or agursoy@ku.edu.tr or okeskin@ku.edu.tr

Emir Demirbas' present address is Department of Chemical and Biological Engineering, Princeton University, Princeton, New Jersey.

Editor: Jianhan Chen

https://doi.org/10.1016/j.bpj.2026.01.053

© 2026 The Author(s). Published by Elsevier Inc. on behalf of Biophysical Society.
This is an open access article under the CC BY-NC-ND license (http://creativecommons.org/licenses/by-nc-nd/4.0/).

Please cite this article in press as: Demirbas et al., G12 mutations rewire allosteric communication at the Ras–RalGDS interface, Biophysical Journal (2026), https://doi.org/10.1016/j.bpj.2026.01.053

I can exist in two conformations: state 1 (open), which inhibits effector binding, and state 2 (closed), which favors effector binding and GTP hydrolysis to GDP (8).

Three major Ras isoforms, H-Ras, N-Ras, and K-Ras, are mutated in more than 20% of human cancers; thus, they have been the subject of extensive oncogenic research (9). Around 94% of these mutations are observed at three specific hotspots: G12, G13, and Q61 (10). It has been demonstrated that these mutations disrupt the GTP hydrolysis activity of Ras, leading to a persistent active state that enhances downstream signaling (11,12). K-Ras is the most frequently mutated isoform in human cancers, and its mutations are prevalent in pancreatic, colorectal, and lung adenocarcinomas. In contrast, H-Ras mutations are less common and are primarily observed in head and neck, thyroid, and bladder adenocarcinomas (9). N-Ras mutations are also less common but are more frequent in melanoma.

The best-characterized Ras signaling pathways are the Ras/MEK/ERK and PI3K/AKT/mTOR cascades, although the Ras/RalGDS/Ral pathway has gained increased attention over the last decade (13). Ral (Ras-like) GTPases display a high sequence similarity with Ras GTPases and were initially identified in Ras-related oncogene research (14). The two isoforms of Ral are RalA and RalB (13). Ral-effector interactions regulate multiple cellular events, including actin cytoskeleton rearrangement, cell motility, and proliferation, and their aberrant activity leads to metastasis and invasion (15–18). Recently, Cao et al. (19) showed that Ral GTPases are highly active in pancreatic ductal adenocarcinoma (PDAC) and contribute to its aggressive nature by increasing TGF-β1, transforming growth factor-β1, production. Furthermore, Neel et al. (20) provided the first description of invadopodia formation in PDAC cells, which is known to affect metastatic and invasive behavior in other cancer types. They suggested that invadopodia formation is dependent on the mutant K-Ras^{G12V} activity and RalB but not on the Raf effector pathway. In a separate study, Ghoroghi et al. (15) demonstrated that RalA and RalB promote breast cancer metastasis in the lungs by controlling the properties of exosomes, which are crucial for forming pre-metastatic niches.

Ral GTPases, like Ras, also cycle between a GTP-bound active and a GDP-bound inactive state (13). Their intrinsic GTP hydrolysis activity is weak; therefore, it needs to be facilitated by Ral-selective GTPase-activating proteins (RalGAPs) (21). On the other hand, their activation relies on Ral-selective guanine nucleotide exchange factors (RalGEFs), which can activate Ral in a Ras-dependent or independent manner (22). So far, seven different RalGEFs have been identified: Ral guanine nucleotide dissociation stimulator (RalGDS), RalGEFs with pleckstrin homology (PH) domain and SH3 binding motif (RalGPS, isoforms 1 and 2), and RalGDS-like (RGL, isoforms 1, 2, 3, and 4) (13). Different Ras family members can activate RalGDS, RGL1, RGL2, and RGL3, whereas activations of RalGPS1, RalGPS2, and RGL4 are Ras independent (17). All RalGEFs are multidomain proteins and share a common domain architecture: A Ras exchanger motif (REM) located in the N-terminal region, a central Cdc25 homology domain for their catalytic activity, and an RBD in the C-terminal region, which is only present in Ras-dependently activated RalGEFs (22). Upon stimulation of RBD by GTP-bound Ras proteins, the catalytic Cdc25 domain regulates the conversion of the GDP-bound state to the GTP-bound state of Ral GTPases (23).

It was thought that the Raf and PI3K effector pathways were sufficient to explain Ras-driven tumor progression. However, mounting evidence shows that the Ras/RalGDS/Ral pathway is also critical for Ras-driven tumorigenesis of human cells (18,24–26). RalGDS functions as a bridge between Ras and Ral. Ras proteins recruit RalGDS to the plasma membrane, where they become proximal to Ral proteins, which is thought to be sufficient for the activation of Ral by RalGDS (23). Ras and RalGDS RBD form an antiparallel β-sheet extension via the β2-strands from both Ras and RalGDS RBD. The charged side-chain interactions further stabilize the β-sheet. Ras β2-strand corresponds to the switch I region that is known to be responsible for recognition of the RBD of its effectors, such as RalGDS (27). The activation mechanism of RalGDS is controlled by several Ras family members, including K-Ras, H-Ras, M-Ras, and Rap1, but not by other family members such as Rab and Rho (28–32). Two major isoforms, K-Ras and H-Ras, have 100% sequence identity in their effector lobe (Fig. 1). M-Ras is a member of the R-Ras subgroup and a close relative of K-Ras, H-Ras, and N-Ras. M-Ras and K-Ras show 53% amino acid identity (33). Rap1, another close relative of Ras isoforms, is known as a Ras antagonist (34). Experimental studies have revealed that H-Ras, K-Ras, M-Ras, and Rap1 exhibit distinct binding affinities to the RalGDS RBD. Rap1–RalGDS interaction is the tightest interaction seen in the Ras family members, whereas M-Ras is the weakest (35,36). The binding affinities of H-Ras and K-Ras to the RalGDS RBD are intermediate, higher than that of M-Ras but lower than that of Rap1 (37). Despite the high-affinity interaction between Rap1 and RalGDS, Ral activation was not detected upon Rap1-induced RalGDS activation (31), which is attributed to the different localizations of Rap1 and Ral (38). Therefore, it is thought that Rap1 may have an inhibitory effect on RalGDS/Ral signaling, rather than activation, which is consistent with its role as a Ras antagonist.

To investigate Ras-initiated metastasis activity, Yin et al. (24) assayed tumorigenesis in the DU145 cell line (a human prostate cancer cell line with low metastatic activity) infected with retroviruses expressing the H-Ras protein with the G12V mutation. They reported that RalGDS activation is essential for bone metastatic activity by showing that impaired RalGDS/Ral interaction reduced metastasis by 65%. In addition, Tchevkina et al. (18) noted that H-Ras

Please cite this article in press as: Demirbas et al., G12 mutations rewire allosteric communication at the Ras–RalGDS interface, Biophysical Journal (2026), https://doi.org/10.1016/j.bpj.2026.01.053

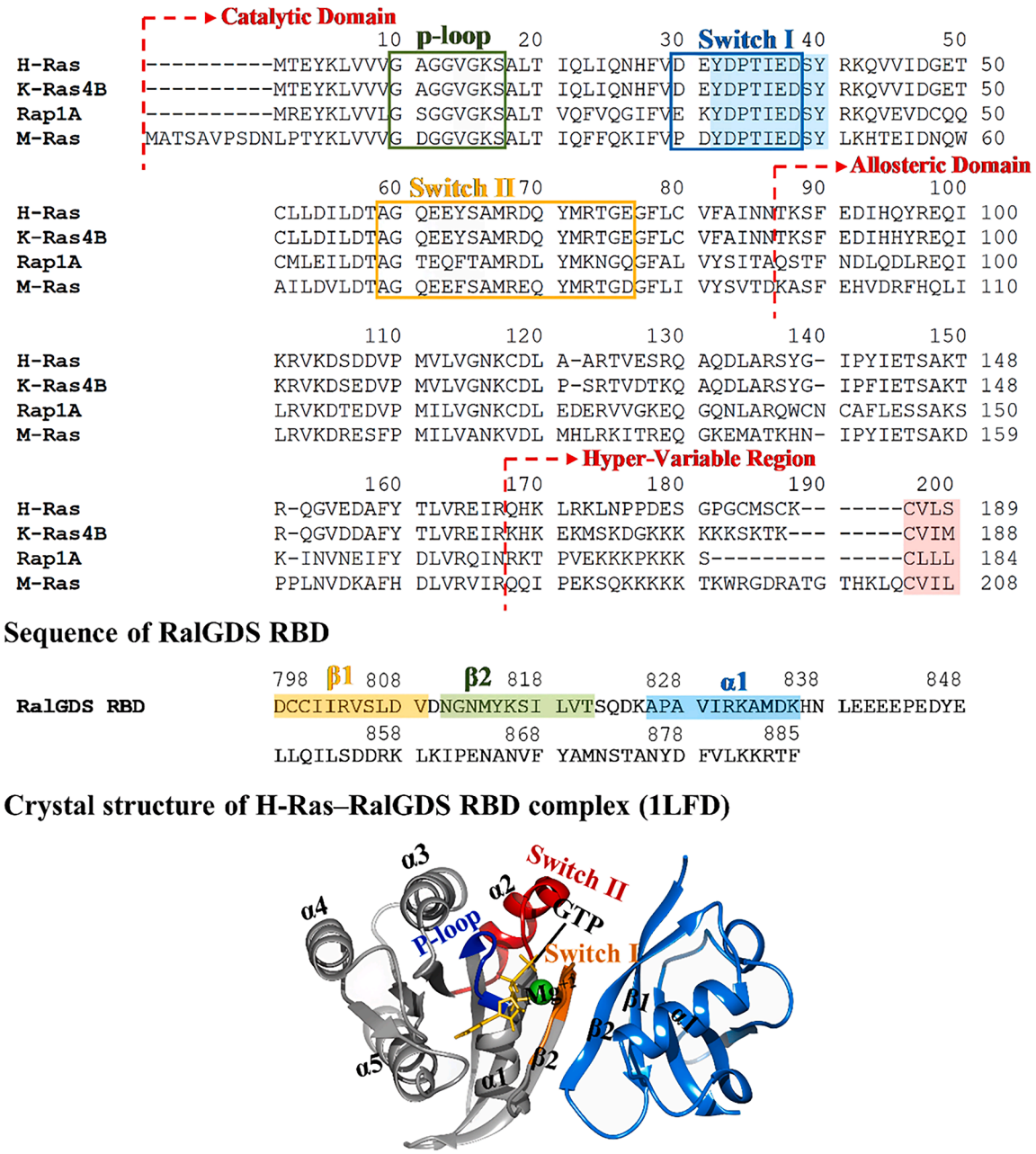


FIGURE 1 (Top) Sequence alignment of closely related Ras family members H-Ras, K-Ras4B, Rap1A, and M-Ras. GEF, GAP, effector binding, and nucleotide binding regions are labeled as switch I, switch II, and P-loop, respectively. Beginning of the catalytic domain, allosteric domain, and hypervariable region are marked with red arrows. The effector binding loop is highlighted in blue, and the CAAX motif is highlighted in pink. (Middle) Sequence of RalGDS RBD. Secondary structure elements that participate in Ras binding are highlighted in yellow, green, and blue. (Bottom) Crystal structure of H-Ras-RalGDS RBD complex (PDB: 1LFD). H-Ras (*gray*)-RalGDS (*blue*) representative complex. Secondary structure elements are labeled: switch I, orange; switch II, red; P-loop, blue.

significantly stimulates spontaneous metastatic activity through the Ras/RalGDS/RalA signaling pathway.

Although experimental studies have highlighted the involvement of RalGDS in cancer development and progression, the dynamic behavior of Ras-RalGDS RBD interaction remains unexplored. Here, we carried out long-timescale molecular dynamics (MD) simulations to gain detailed insight into how the interactions between Ras and RalGDS differ among Ras family members. Previously, we observed that using multiple conformations of Ras proteins makes it possible to find a suitable conformation that fits the drug molecule or their effectors (39). Furthermore,

Please cite this article in press as: Demirbas et al., G12 mutations rewire allosteric communication at the Ras–RalGDS interface, Biophysical Journal (2026), https://doi.org/10.1016/j.bpj.2026.01.053

the effect of oncogenic G12D and G12V mutations on K-Ras4B–RalGDS and H-Ras–RalGDS interactions was investigated. Binding free energy results showed that Rap1–RalGDS indeed has the tightest interaction among the selected isoforms, while M-Ras–RalGDS has the weakest. It was observed that Ras uses the same interface residues while binding to RalGDS and Raf. Bonding profiles revealed differences in interaction preferences in mutant systems along with several conserved interactions that ensure complex stability. We also uncovered how allosteric communication is altered upon G12D/V mutations. Overall, the mechanistic differences revealed by this work are crucial for developing effective treatment strategies, particularly for cancer types that exhibit aggressive metastatic behavior through the Ral pathway.

MATERIALS AND METHODS

Simulation systems and initial configuration preparation

To resolve Ras–RalGDS interaction dynamics, a total of eight simulation systems, namely K-Ras4B^{WT}, K-Ras4B^{G12D}, K-Ras4B^{G12V}, H-Ras^{WT}, H-Ras^{G12D}, H-Ras^{G12V}, M-Ras^{WT}, and Rap1^{WT} in complex with RalGDS RBD, were generated. The initial coordinates for RalGDS RBD, K-Ras4B, H-Ras, M-Ras, and Rap1 were adopted from the following crystal structures: RalGDS RBD in complex with H-Ras^{WT} (PDB: 1LFD), K-Ras4B^{WT} in complex with RGL1 (PDB: 7SCW), K-Ras4B^{G12D} in complex with natural product-like compound 9b (PDB: 6QUW), K-Ras4B^{G12V} in complex with RGL1 (PDB: 7SCX), M-Ras^{D41E} (PDB: 3PIT), and Rap1 in complex with KRIT1 (PDB: 4DXA) (Table S1). We employed the crystal structure of H-Ras–RBD complex as a template for constructing model complexes with other GTPases using PRISM (40). The initial configurations for the simulated systems are shown in Fig. S1. For the H-Ras^{WT}–RBD complex, the initial coordinates were directly adopted from 1LFD. For both H-Ras^{G12D}–RBD and H-Ras^{G12V}–RBD complexes, mutant H-Ras systems were derived from the wild-type (WT) structure by in silico mutagenesis. To construct the initial configuration of the K-Ras4B^{WT}–RBD complex, the catalytic domain of K-Ras4B was superimposed onto H-Ras in complex with RalGDS RBD. Similarly, both K-Ras4B mutants in PDB: 6QUW and PDB: 7SCX were superimposed onto the RBD-bound H-Ras, generating the coordinates of the K-Ras4B^{G12D}–RBD and K-Ras4B^{G12V}–RBD complexes, respectively. Likewise, the crystal structures of M-Ras and Rap1 were superimposed onto the RBD-bound H-Ras, generating the coordinates of the M-Ras–RBD and Rap1–RBD complexes. The M-Ras D41E mutation was converted to WT. For all GTPases, GTP analogs in the crystal structures, such as GNP, GCP, and GSP, were converted to GTP, while Mg^{2+} was maintained intact. Missing loops in some GTPases were modeled using Chimera MODELLER (41).

Atomistic MD simulations

We generated eight different initial configurations of the RalGDS RBD in complex with Ras and Rap1 proteins (Fig. S1). The initial configurations were subject to MD simulations using the CHARMM program with the updated all-atom additive force field (version 36) (42,43). To optimize the dimeric interface, a series of minimization cycles using steepest descent (1200 steps) followed by adopted basis Newton-Raphson (600 steps) were performed for the complex systems. All simulations were performed in an aqueous environment, using the TIP3P water model to solvate the system. The protein complex was placed in a periodic, isometric unit cell box of $90 \times 90 \times 90$ Å^3, which yields almost 75,000 atoms. To achieve a total cation concentration of approximately 100 mM, which mimics physiological conditions, 40 Cl^- were added to all systems. Depending on the total charge, 50–55 Na^+ were added to neutralize the systems. Prior to the production runs, a series of minimization and dynamics cycles was performed for the solvents, including ions surrounding the harmonically restrained protein backbone in the complex, until the solvent temperature reached 310 K. Each complex was energy minimized for 10,000 steps. Dynamics runs were executed under isothermal-isobaric (NPT) ensemble with a 2-fs time step. During pre-equilibration, the harmonic constraints on the protein backbone were gradually removed by reducing the force constant from 5 to 1 kcal/mol/Å^2/atom. The production runs were performed at a constant pressure of 1 atm (1.01325 bar), maintained by the Nosé-Hoover Langevin pressure control (44), and at a constant temperature of 310 K, maintained by the Langevin thermostat. The local interaction distance cutoff was set to 12 Å to control van der Waals interactions. A smoothing function was used with a switch distance of 10 Å. Long-range electrostatic calculations were performed using the particle mesh Ewald method (45). The SHAKE algorithm was applied to constrain the motions of the bonds that involve hydrogen atoms. Each system was simulated for 1 μs using the NAMD package (version 2.14) (46). Furthermore, two additional independent 1-μs simulations were performed for each system to verify reproducibility. Simulations were performed on the Biowulf cluster at the National Institutes of Health (Bethesda, MD) and the Koc University Advanced Computing Cluster (KUACC) (Istanbul, Turkey).

Binding free energy calculations

Binding free energy is a useful quantity to compare relative binding affinities across eight systems. It can be estimated using molecular mechanics (MM) combined with the generalized Born (GB) and surface area continuum solvation (MM/GBSA) method (47). In the MM/GBSA method, the binding free energy is separated into two terms: gas-phase solute energy, whose components are approximated by the MM methods, and the solvation energy, which is a sum of both electrostatic and nonpolar contributions. Binding free energies are then computed as the difference between the complex and the separated receptor (Ras) and ligand (RBD) energies extracted from the same trajectory. Therefore, this method assumes that contributions from solvation changes and conformational differences between the free and bound states are negligible, and it focuses on interfacial interactions. To obtain a more accurate estimate of the binding free energy, a common approach is to calculate the conformational entropy term. The entropy contribution to the binding free energy is further divided into three components: translational, rotational, and vibrational contributions. These terms can be calculated by quasiharmonic approximation (48,49). All calculations described above were carried out using the mmpbsa.py script in the Amber17 program with default parameters (50,51). ParmEd was used to convert CHARMM parameter and topology files into Amber-compatible format (52). The Mbondi2 radii set was used as atomic radius parameters (53). All water molecules and ions were stripped off before MM/GBSA calculations, and Cα atoms-only trajectories were used for entropy calculations in order to avoid noise caused by side-chain fluctuations.

RMSD, RMSF, and bond analysis

To determine how much the protein conformation has changed between two time points and ensure that the system reaches equilibrium, checking the root-mean-square deviation (RMSD) value is one method. To calculate the RMSD, translational and rotational motions were removed from the trajectory. Moreover, root-mean-square fluctuation (RMSF) per residue was calculated to identify the most flexible regions. The MDTraj library was used to compute both RMSD and RMSF (54). Bond profiles were analyzed to detect isoform-specific interactions. The Hydrogen Bonds plug-in of VMD (55) was used to calculate hydrogen bonds (H bonds) with a

Please cite this article in press as: Demirbas et al., G12 mutations rewire allosteric communication at the Ras–RalGDS interface, Biophysical Journal (2026), https://doi.org/10.1016/j.bpj.2026.01.053

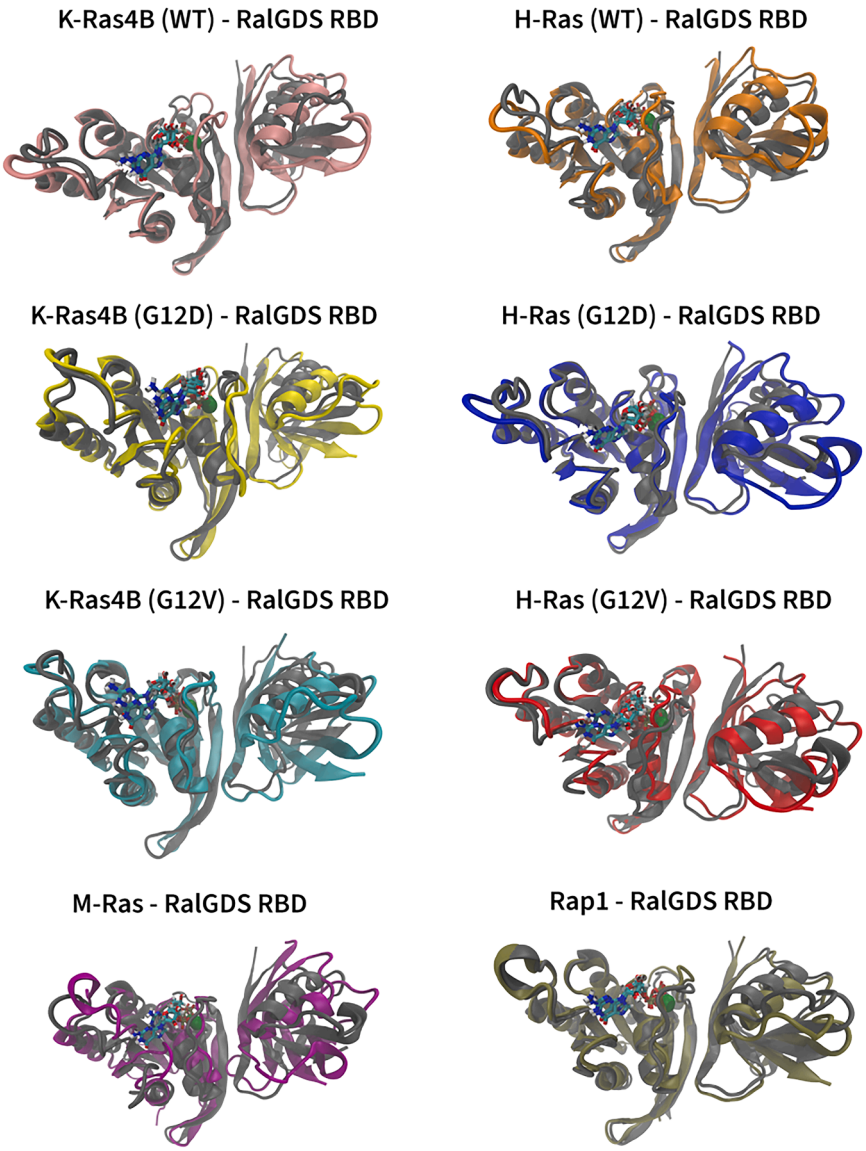


FIGURE 2 Superimposition of initial and final conformations. All initial conformations of K-Ras4B (WT and its mutants), H-Ras (WT and its mutants), M-Ras, and Rap1 in complex with RalGDS RBD are shown in light gray. Superimposed final conformations are shown in various colors: pink, yellow, cyan, orange, dark blue, red, purple, and tan.

donor-acceptor distance cutoff of 3.5 Å and an angle cutoff of 30°. Next, the interactions between the cationic (Lys and Arg) and anionic (Asp and Glu) residues through the side chains were classified as salt bridges, the interactions between Tyr and charged residues were classified as cation/anion-π, and the rest were classified as H bonds, depending on the involved atoms. The Salt Bridges plug-in of VMD was then used to validate the salt bridges using a distance criterion of 3.5 Å. In this way, we define salt bridges as directional, charge-assisted H bonds, following Bosshard et al. (56) and Donald et al. (57). Throughout the 1-μs trajectory, H bonds and salt bridges with occupancy 20% or above across three replicas were considered stable. All residues that contributed to bond formations were further analyzed to distinguish differences between the WT and mutant systems.

Clustering, network, and residue cross-correlation analyses

Production run trajectories were clustered based on the RMSD values using the *k*-means algorithm in Amber17 (50), and the top three cluster representatives were further analyzed. Allosteric communication networks are crucial for a protein's function, as they facilitate the transmission of a signal from one region to another distant one. We used PSNtools (58) to calculate the residue-level interaction networks and the metapaths within each complex. The outputs were analyzed using in-house Python scripts. The CORMAN module of the CHARMM program was used to calculate positional dynamic cross-correlation matrices (DCCMs) (43). Only Cα atoms were used in DCCM calculations, as they are sufficient to describe large system motions.

RESULTS

We performed long-timescale all-atom MD simulations on RalGDS RBD in complex with K-Ras4B, H-Ras, M-Ras, and Rap1 in an aqueous environment. For both K-Ras4B and H-Ras, two oncogenic mutants, G12D and G12V, were also simulated with the RBD of RalGDS. During the simulations, we did not observe dissociation of Ras and RBD (Fig. 2). Additionally, GTP remained bound to Ras throughout the simulations without being hydrolyzed, as

Please cite this article in press as: Demirbas et al., G12 mutations rewire allosteric communication at the Ras–RalGDS interface, Biophysical Journal (2026), https://doi.org/10.1016/j.bpj.2026.01.053

expected. RMSD and RMSF profiles of the replica simulations are given in Fig. S2. An interesting observation is that the third replica of the H-Ras^{G12V} system undergoes high RMSD fluctuations. Possible explanations for this are discussed in the following sections. The RMSD profiles of the complexes from the first set of simulations are given in Fig. S3.

The structure of RBD is highly homologous among Ras effectors (Fig. S4). It contains five β-strands and two α-helices. In the interaction with GTPases, its β2-strand forms an extended β-sheet with the β2-strand of GTPases through the intermolecular backbone H bonds. The β-sheet extension stabilizes the dimeric interface. Additionally, side-chain interactions between the α1-helix and the catalytic domain of GTPases further stabilize the complex formation. Below, we provide atomic-level insight into the binding mechanism of Ras–RalGDS RBD interaction.

Switch I and switch II regions of the Ras family members reveal distinct fluctuation profiles when interacting with RalGDS RBD

Production run trajectories were clustered based on RMSD values. The top three cluster coverages are shown in Fig. S5. No major conformational shifts were observed between the highly populated clusters except for fluctuation differences in switch I and switch II regions of Ras (Fig. S6). RMSF calculations showed that K-Ras4B, H-Ras, M-Ras, and Rap1 proteins exhibit differential fluctuations in their interactions with RalGDS RBD (Fig. 3 *A*). In particular, high flexibility is observed in the switch regions. Rap1 has the most flexible switch I region and the least flexible switch II region. Conversely, M-Ras exhibits the least flexibility in the switch I region, with the highest flexibility in the switch II region. Significant fluctuations in the switch II region of M-Ras might be the reason for low binding affinity toward RalGDS RBD (see below). Despite 100% sequence identity, K-Ras4B^{WT} is more flexible than H-Ras^{WT} in both regions, in line with previous computational studies (59–61). G12D/V mutations slightly decreased the flexibility of switch II in both the K-Ras4B (Fig. 3 *B*) and H-Ras (Fig. 3 *C*).

Binding free energy calculations qualitatively reproduce the experimental binding hierarchy for WT systems

Binding free energies were calculated for all eight systems (Fig. 4 *A*). Our binding free energy results show that, among the WT systems, Rap1–RBD interaction is the strongest with -55.5 ± 2.2 kcal/mol among the studied Ras family members, whereas M-Ras–RBD is the weakest with -36.0 ± 2.4 kcal/mol. K-Ras4B^{WT} and H-Ras^{WT} showed comparable binding affinities with -48.3 ± 0.1 kcal/mol and -46.1 ± 1 kcal/mol, respectively. For the WT K-Ras4B, H-Ras, M-Ras, and Rap1 systems, our calculated values exhibit the profiles of binding affinities in qualitative agreement with the experimental results (Fig. 4 *B*). Despite systematic overestimation of absolute binding free energies, the computational results reproduce the experimental ordering ($R^2 = 0.74$ and Spearman's $\rho = 0.80$). K-Ras4B mutant systems were largely insensitive to the mutations, with similar binding free energies across three systems. In contrast, H-Ras mutant systems exhibited a different profile. Although the calculated binding free energies for the K-Ras4B and H-Ras complexes overlap within the error ranges, a high degree of variability was observed for H-Ras^{G12V}. This was primarily due to the third replica, which exhibited a low binding free energy of -10.6 kcal/mol (Table S2). This can be attributed to the low occupancies of critical Asp33^{Ras}–Lys836^{RBD} and Arg41^{Ras}–Gly812^{RBD} interactions, which contribute to the stability of the complex (see below). Entropic loss upon complex formation seems to be similar among the isoforms, which is expected. The main affinity differences are introduced by enthalpic contributions, with the minimum being -76.8 ± 5 kcal/mol for the M-Ras system and the maximum -104.7 ± 2.2 kcal/mol for the Rap1 system.

In Ras–RBD interaction, conserved Arg41^{Ras}–Gly812^{RBD}, Ser39^{Ras}–Tyr815^{RBD}, Glu37^{Ras}–Ser817^{RBD}, Glu37^{Ras}–Tyr815^{RBD}, and Asp33^{Ras}–Lys836^{RBD} pairs act as a scaffold, and G12 mutations favor Glu37-mediated stabilization

Overall, the effector region of Ras is acidic. Glu31, Asp33, Glu37, and Asp38 create a negatively charged binding site for positively charged complementary amino acids of RalGDS RBD with Arg804, Lys816, and Lys836. In the simulations, we observed that the Arg41^{Ras}–Gly812^{RBD}, Ser39^{Ras}–Tyr815^{RBD}, and Glu37^{Ras}–Ser817^{RBD} H bonds and Glu37^{Ras}–Tyr815^{RBD} anion-π interaction are conserved in all systems except for M-Ras, with varying occupancies (Tables S3–S6). The Asp33^{Ras}–Lys836^{RBD} (Asp43^{Ras}–Arg804^{RBD} for M-Ras) salt bridge is strongly conserved across all systems, including M-Ras. These interactions act as a scaffold and seem to be responsible for the complex integrity (Fig. 5, *A* and *B*). It should be noted that slightly lower average occupancies and higher variabilities of Asp33^{Ras}–Lys836^{RBD} and Arg41^{Ras}–Gly812^{RBD} interactions in H-Ras^{G12V} can be attributed to low occupancies of these interactions in the third replica, which in turn caused high RMSD fluctuations and decreased the binding affinity, as discussed above (Figs. S2 and 4A). Glu37^{Ras}–Arg804^{RBD} (Glu47^{Ras}–Arg804^{RBD} for M-Ras) is also seen in all systems; however, lower occupancies and high variabilities in some systems suggest that this is a transient interaction.

The salt bridge of Asp33^{Ras}–Lys836^{RBD} acts like a clamp in the distant region of the β-sheet interface and reaches particularly high occupancies in mutant K-Ras4B systems

Please cite this article in press as: Demirbas et al., G12 mutations rewire allosteric communication at the Ras–RalGDS interface, Biophysical Journal (2026), https://doi.org/10.1016/j.bpj.2026.01.053

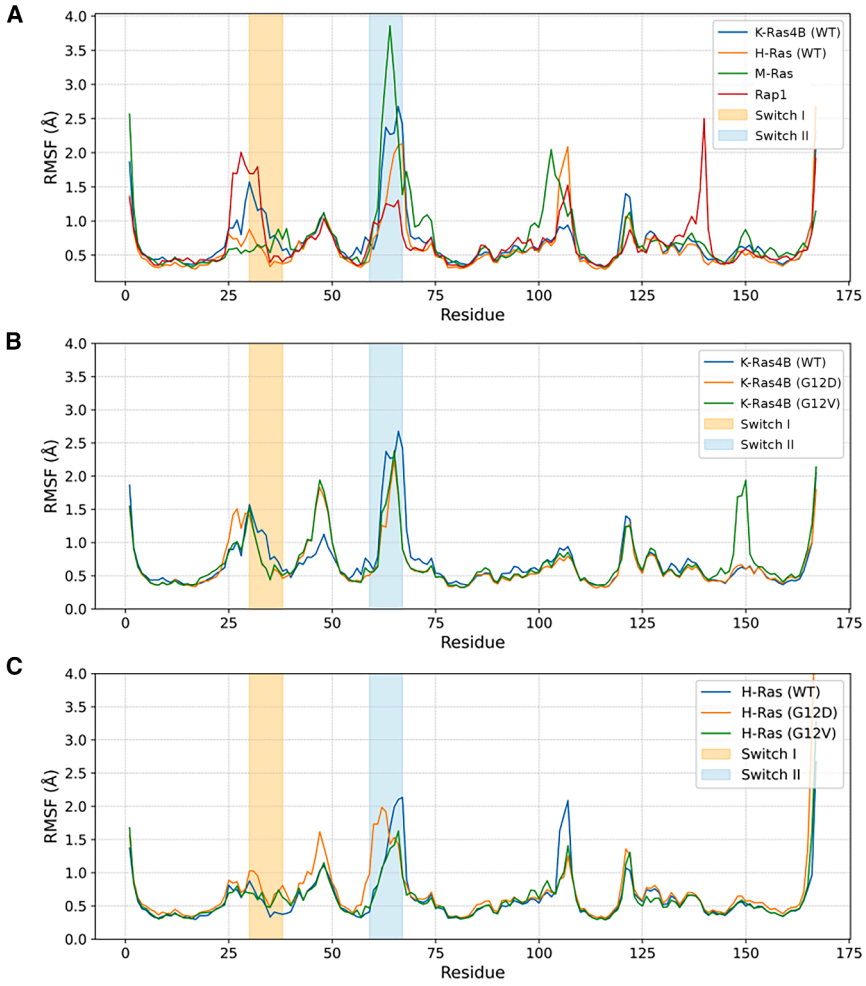
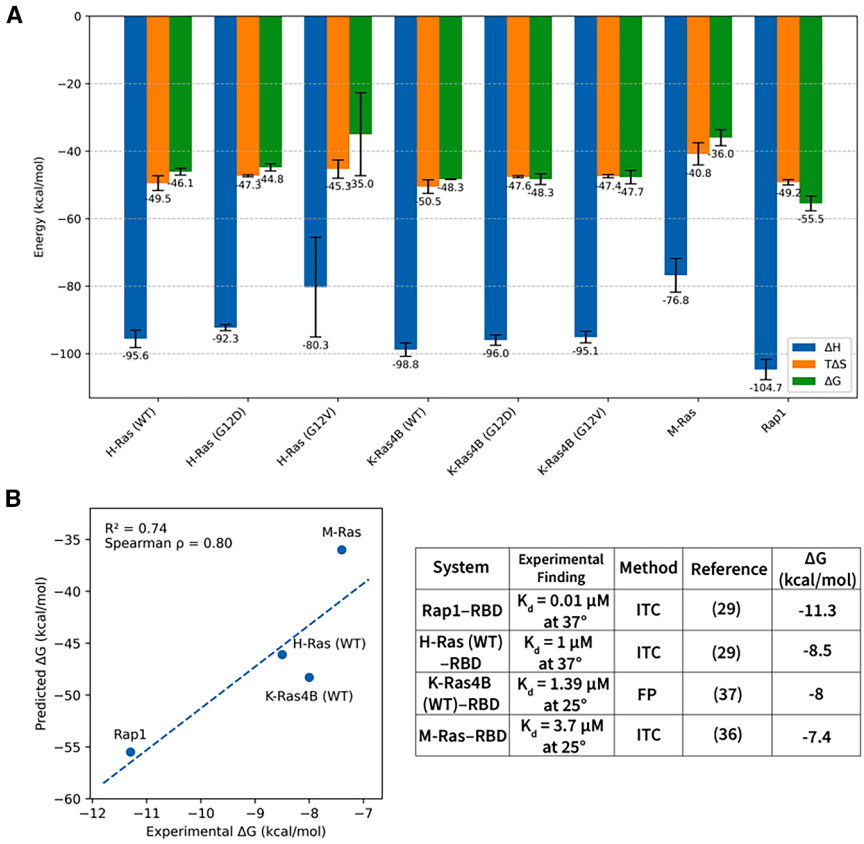


FIGURE 3 Cα RMSF of Ras monomers. In each graph, the x axis shows the residue number, and the y axis indicates the corresponding RMSF value. The switch I (30–38) and switch II (59–67) regions are labeled and highlighted with yellow and light blue, respectively. (*A*) RMSF comparison of all wild-type systems. K-Ras4B^{WT} is colored dark blue, H-Ras^{WT} orange, M-Ras green, and Rap1 red. (*B*) RMSF comparison of K-Ras4B systems. K-Ras4B^{WT} is colored dark blue, K-Ras4B^{G12D} orange, and K-Ras4B^{G12V} green. (*C*) RMSF comparison of H-Ras systems. H-Ras^{WT} is colored dark blue, H-Ras^{G12D} orange, and H-Ras^{G12V} green.

(Fig. 5 *B*). Asp38^{Ras} (Asp48^{Ras} for M-Ras) is another critical hotspot, as it forms salt bridges with various residues (Ser817^{RBD}, Lys816^{RBD}, and Lys836^{RBD}) in the RalGDS RBD in each system, suggesting that this residue persistently contributes to the interaction (Fig. 5 *C*). In the H-Ras^{WT} system, it forms interactions with Lys816^{RBD} and Ser817^{RBD}. In the presence of G12 mutations, these interactions are weakened; however, the interactions between Glu37^{Ras}–Ser817^{RBD} and Glu37^{Ras}–Tyr815^{RBD} are strengthened (Fig. 6). This observation suggests that Glu37 and Asp38 act as a mutation-sensitive pair within switch I, and that G12 mutations favor stabilization through Glu37. Complete loss of Asp38^{Ras}–Ser817^{RBD} H bond in H-Ras^{G12V} is likely compensated by the formation of Asp38^{Ras}–Lys836^{RBD} salt bridge, as it is only seen in the H-Ras^{G12V} system.

In K-Ras4B systems, the picture resembles that of H-Ras systems. Again, upon G12 mutations, Glu37^{Ras}–Ser817^{RBD} and especially Glu37^{Ras}–Tyr815^{RBD} interactions are strengthened, underscoring the role of Glu37 in mutant systems (Fig. 6). Also, the anion-π interaction between Glu37^{Ras} and Tyr815^{RBD} seems crucial in all mutant systems. In contrast to H-Ras^{WT}, in the K-Ras4B^{WT} system, Asp38^{Ras} forms salt bridges with both Lys816^{RBD} and Lys836^{RBD}; however, these interactions are not observed simultaneously due to the distal location of the Lys residues (Fig. 5 *C*). However, interestingly, K-Ras4B mutants completely lost Asp38^{Ras}–Lys816^{RBD} contact; Asp38^{Ras} preferentially interacts with Lys836^{RBD} in these systems. Additionally, the presence of the Asp38^{Ras}–Lys836^{RBD} interaction appears to prevent the formation of a persistent Asp38^{Ras}–Ser817^{RBD} interaction, evidenced by low occupancies in K-Ras4B$^{G12D/V}$. This is mainly because the same side-chain oxygen of Asp38^{Ras} is involved in both interactions (Fig. 5 *C*). Another striking observation is that the Pro34^{Ras}–Lys836^{RBD} H bond is only seen in K-Ras4B systems. However, this interaction does not appear to contribute significantly to complex integrity, since the K-Ras4B and H-Ras systems have similar binding affinities for the RalGDS RBD (Fig. 4 *A*).

According to binding free energy results, the M-Ras–RBD complex is the least stable among all systems, and its interaction profile explains this situation. Glu37^{Ras}–Ser817^{RBD}



System	Experimental Finding	Method	Reference	ΔG (kcal/mol)
Rap1–RBD	K_d = 0.01 μM at 37°	ITC	(29)	-11.3
H-Ras (WT) –RBD	K_d = 1 μM at 37°	ITC	(29)	-8.5
K-Ras4B (WT)–RBD	K_d = 1.39 μM at 25°	FP	(37)	-8
M-Ras–RBD	K_d = 3.7 μM at 25°	ITC	(36)	-7.4

FIGURE 4 Binding free energy analysis. (*A*) Binding free energy decomposition of Ras–RalGDS complexes. The *x* axis displays the system names, and the *y* axis represents the corresponding energy values. ΔH, $T\Delta S$, and ΔG values are represented in kcal/mol by blue, orange, and green bars, respectively. The enthalpic contribution is calculated by MM/GBSA, and the entropic contribution is calculated by quasiharmonic approximation. Data are presented as mean ± SEM. (*B*) Qualitative agreement between experiment and predictions. A linear regression is shown to guide the eye. MM/GBSA systematically overestimates the absolute binding free energies; therefore, results are interpreted qualitatively. Experimental K_d values are provided, along with the corresponding experimental method, reference, and binding free energy values. Experimental binding free energies are calculated using the relation $\Delta G = RT\ln K_d$.

(Glu47^{MRas}–Ser817^{RBD} for M-Ras) and Ser39^{Ras}–Tyr815^{RBD} (Ser49^{Ras}–Tyr815^{RBD} for M-Ras) H bonds and Glu37^{Ras}–Tyr815^{RBD} (Glu47^{MRas}–Tyr815^{RBD} for M-Ras) anion-π interaction are observed in all systems except M-Ras–RBD (Table S5). In addition, unlike the other systems, which contain Arg41, M-Ras contains Leu51 at this position. Both residues are capable of forming an H bond with Gly812^{RBD}, yet the Arg41^{Ras}–Gly812^{RBD} H bond is more persistent than the Leu51^{Ras}–Gly812^{RBD} H bond, due to the presence of the guanidinium group, which is a strong H-bond donor, in arginine. On the other hand, leucine can only form an H bond through backbone atoms. In our previous study, we had observed that the R41E/K42D double mutations in G12D mutants of K-Ras4B almost completely influenced mRNA levels of ERK- and Akt-regulated genes (62). The interaction profiles of K-Ras4B^{WT} and Rap1 are fairly similar except for the Lys31^{Rap1}–Asp835^{RBD} salt bridge, which is only present in the Rap1 system (Fig. 5 *D* and Table S6). Considering the interaction strength between Rap1 and RBD, Lys31^{Rap1} appears to be the key factor in amplifying the stability. It should be noted that all other systems contain an Asp or a Glu in the 31st residue. Additionally, given the residue locations, the salt bridge between the Lys31^{Rap1}–Asp835^{RBD} salt bridge serves as a second clamp for the interaction, similar to the one between Asp33^{Ras} and Lys836^{RBD}. Also, the Asp38^{Rap1}–Ser817^{RBD} H bond is more persistent in Rap1 compared to other systems.

Network analysis offers insights into how allosteric communication varies across different complexes

To verify whether switch I of Ras remained in state 2, which favors effector binding, throughout the trajectories, we calculated the distance between Thr35^{Ras} and γ-phosphate of GTP following our previous work (63). It can be seen that the distances are concentrated between 4 and 7 Å (Fig. S7), so all H-Ras and K-Ras4B complexes remained in state 2, as expected. However, different switch I states are generally defined for the monomeric Ras, before effector binding, since the β2-strand engages to form a stable, extended β-sheet with the effector upon binding. Therefore, we examined allosteric communication networks to elucidate isoform-specific interaction mechanisms.

We created residue-level interface networks for H-Ras and K-Ras4B systems to examine the differences in the interface between Ras and RalGDS. The interface connections, i.e., edges where one node is from H- or K-Ras4B systems and the other is from the RBD, are presented in Fig. 7. Table 1 summarizes the interface networks. Within each

Please cite this article in press as: Demirbas et al., G12 mutations rewire allosteric communication at the Ras–RalGDS interface, Biophysical Journal (2026), https://doi.org/10.1016/j.bpj.2026.01.053

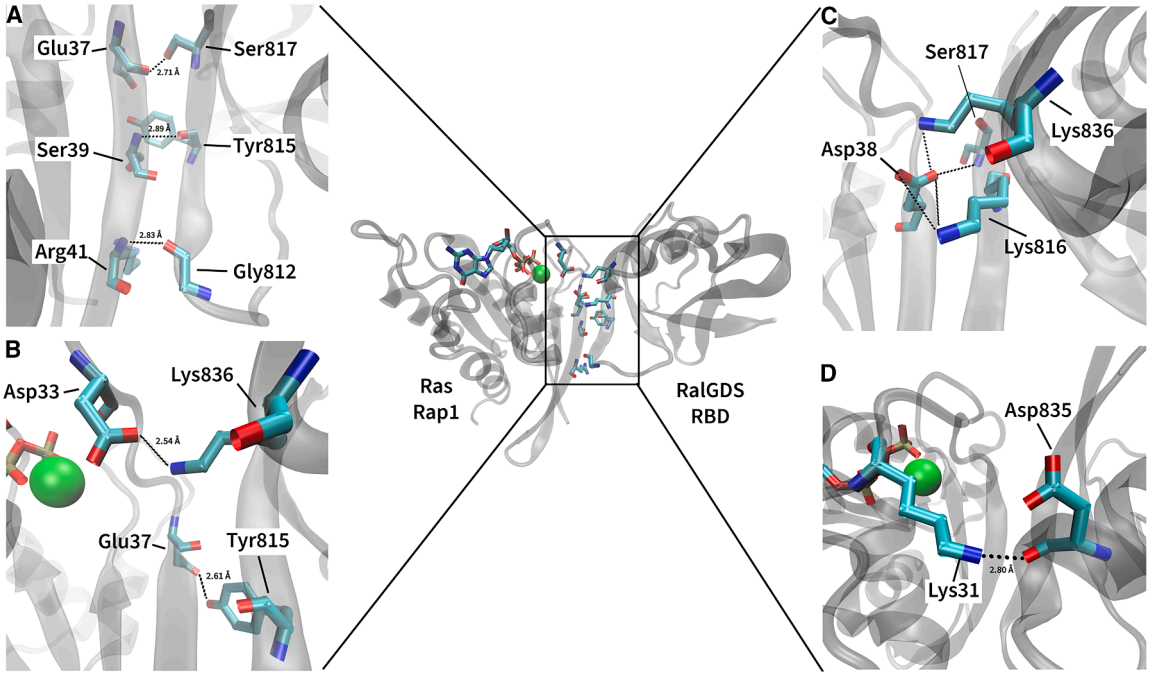


FIGURE 5 Interactions formed between Ras and RalGDS RBD. (*A*) The H bonds Glu37^{Ras}–Ser817^{RBD}, Ser39^{Ras}–Tyr815^{RBD}, and Arg41^{Ras}–Gly812^{RBD} are conserved except for M-Ras. (*B*) The salt bridge Asp33^{Ras}–Lys836^{RBD} and anion-π interaction Glu37^{Ras}–Tyr815^{RBD} are conserved. (*C*) Possible H bonds that can be formed by Asp38^{Ras} in different systems. Distances are not shown, since all the H bonds cannot be formed simultaneously. (*D*) The unique salt bridge Lys31^{Rap1}–Asp835^{RBD} is formed only in Rap1–RBD. Mg^{2+} is shown as a green sphere.

isoform, mutations cause only minor variations in connectivity and node counts. For all systems, the number of Ras and RalGDS nodes is nearly equal. The most significant difference appears between isoforms rather than between mutants. Except for G12V mutants, H-Ras systems have slightly more interface connections than K-Ras4B systems. Again, the third replica for H-Ras^{G12V} caused higher variability seen in H-Ras^{G12V} systems. Additionally, in general, more residues participate in interface connections in H-Ras systems, implying a larger allosteric interaction surface. All systems share four key switch I nodes: Asp33^{Ras}, Ile36^{Ras}, Glu37^{Ras}, and Asp38^{Ras}. There are 14 common interface edges along with seven variable edges in H-Ras systems (Table S7). The edge between Ile36^{Ras}–Ser817^{RBD} is only seen in the mutant H-Ras systems. On the other hand, Asp38^{Ras}–Ser817^{RBD} edge is seen in H-Ras^{WT} but not in H-Ras mutants. K-Ras4B systems share 12 edges, and these overlap strongly with the common edges of H-Ras systems, showing a conserved Ras–RalGDS interface communication network architecture (Table S7). The only edge seen in K-Ras4B mutant systems but not in the WT system is Asp38^{Ras}–Lys836^{RBD}. Similar to H-Ras^{WT}, Asp38^{Ras}–Ser817^{RBD} edge is seen in K-Ras4B^{WT} but not in K-Ras4B mutants.

We also computed the shortest communication pathways within the complexes. Overall, K-Ras4B complexes formed slightly longer and stronger pathways. While H-Ras mutants showed an increase in the number of pathways relative to H-Ras^{WT}, their average path strength did not increase significantly. This implies broader, yet weaker, allosteric communication. In contrast, K-Ras4B mutants had more and stronger pathways, pointing toward stronger and more efficient signal propagation across the dimer. Cross-correlation results also support this finding, as the correlation between the catalytic and allosteric domains increased in mutant systems (Fig. S8). A metapath, which represents a coarse picture of structural communication, was constructed using the most recurrent nodes and edges in the path pool for each complex (Table 2). Metapaths are shown in Fig. S9. Upon mutations, connectivity increased remarkably in K-Ras4B systems, implying more robust signal transduction. In H-Ras systems, while the G12V mutation did not have a significant effect, the G12D mutation reduced connectivity. Across all systems, Ras contributed more to the metapaths, as expected given its larger size relative to RBD.

To uncover specific effects of mutations on allosteric communication, we examined edges involving the 12th residue. We identified the GTP–Gly/Asp/Val12^{Ras}–Gln61^{Ras}–Tyr64^{Ras}–Ile36^{Ras}–Ile803^{RBD} allosteric pathway, which was observed across all systems and connects the active site to the effector through switch regions (Fig. 8 *A*). Edge frequencies suggest a rewiring in this pathway upon G12 mutations (Fig. 8, *B* and *C*). In both WT complexes, Gly12^{Ras} (P-loop) forms a connection with GTP. This coupling supports efficient catalysis in the WT Ras GTPases. However, in oncogenic mutants, the communication between

Please cite this article in press as: Demirbas et al., G12 mutations rewire allosteric communication at the Ras–RalGDS interface, Biophysical Journal (2026), https://doi.org/10.1016/j.bpj.2026.01.053

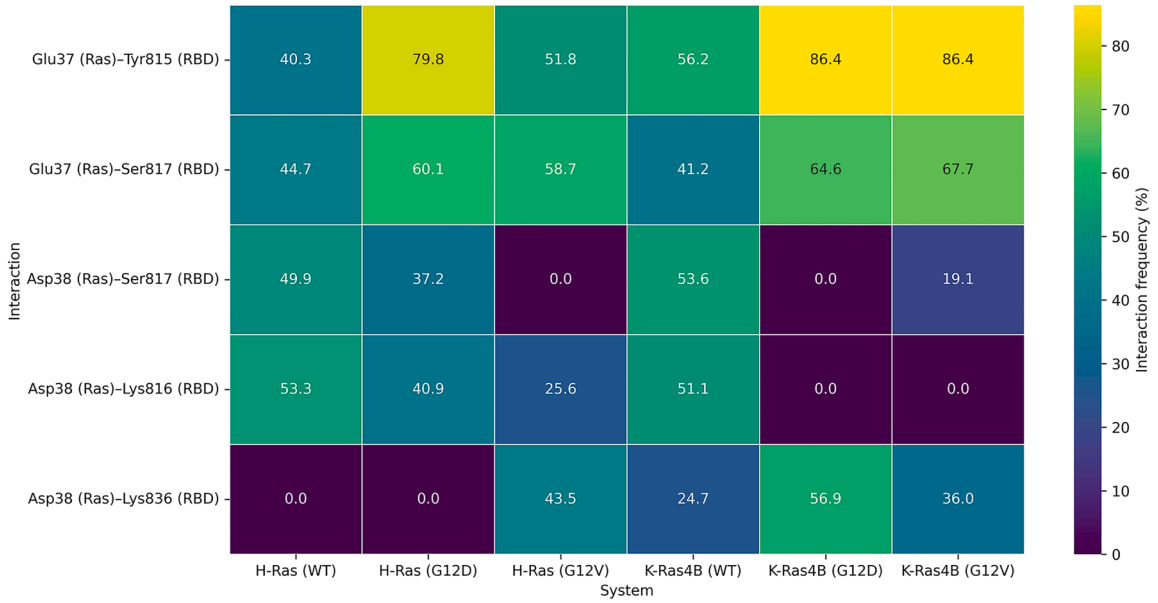


FIGURE 6 Heatmap of Glu37 and Asp38 interaction frequencies in H-Ras and K-Ras4B systems. Average interaction occupancies (%) are shown for wild-type and mutant systems. Glu37 contacts are strengthened, and Asp38 contacts are redistributed upon mutations.

residue 12 and GTP was reduced, while an amplified communication was observed, except for H-Ras^{G12V}, between Asp12^{Ras}/Val12^{Ras} and Gln61^{Ras} (switch II), which is weaker in the WT complexes (Gly12^{Ras}–Gln61^{Ras} for WTs). The link between Gln61^{Ras} and Tyr64^{Ras} transmits the signal within switch II and is more persistent in H-Ras systems. Although it is present in the K-Ras4B systems, relatively high variability suggests that K-Ras4B complexes use alternative paths within switch II. The communication between switch I and switch II seems to be conserved across all complexes through the Tyr64^{Ras}–Ile36^{Ras} link. Furthermore, this link is stabilized by the mutations, especially G12V. Finally, Ile36^{Ras}–Ile803^{RBD} edge connects Ras and RBD in all complexes. This edge is also slightly stabilized in mutant systems relative to WTs. Taken together, we hypothesize that in mutant systems, the reduction in GTP–Gly12^{Ras} and amplification in Asp/Val12^{Ras}–Gln61^{Ras}, Tyr64^{Ras}–Ile36^{Ras}, and Ile36^{Ras}–Ile803^{RBD} communication likely reduce the catalytic activity of Ras GTPases.

DISCUSSION

Ras GTPases are crucial binary switches that participate in multiple pathways affecting cellular growth, gene expression, differentiation, and cytoskeletal organization. Although there is mounting evidence indicating the role of the oncogenic Ras/RalGDS/Ral pathway in cancer development, the interaction between Ras and RalGDS has not been investigated at the atomistic level. For this reason, in this work, we examined structural and dynamical features of Ras–RalGDS RBD complexes using atomistic MD simulations. It should be noted that although the G12 mutations studied here are well-established drivers of human cancer, they operate in a highly mutated cellular landscape (64). Therefore, the structural and dynamic effects reported should be interpreted as biasing oncogenic signaling rather than as sole etiological causes.

Our simulations show that Ras utilizes the identical acidic interface residues when binding to the complementary basic residues of RalGDS RBD and Raf (65). Arg41^{Ras}–Gly812^{RBD}, Ser39^{Ras}–Tyr815^{RBD}, Glu37^{Ras}–Ser817^{RBD}, Glu37^{Ras}–Tyr815^{RBD}, and Asp33^{Ras}–Lys836^{RBD} interactions were identified as essential interactions for a stable Ras–RalGDS RBD interaction, like a scaffold. Furthermore, we demonstrate that Asp38^{Ras} is also crucial for the stability of the complex, as it forms salt bridges with Lys816^{RBD} and Lys836^{RBD}, and an H bond with Ser817^{RBD}. Our binding profiles provide a complementary structural perspective to the experimental works, which previously suggested the stabilizing roles of Asp33^{Ras} and Asp38^{Ras}. Shirouzu et al. (66) demonstrated that the D33A mutation destabilizes the Ras–RalGDS RBD complex, and Linnemann et al. (35) showed that the D38A mutation inhibits Ras–Raf interaction and also weakens Rap1–RalGDS RBD interaction. We propose that the presence of the Lys31^{Rap1}–Asp835^{RBD} salt bridge is the key interaction that amplifies the stability of the Rap1–RalGDS RBD complex. Huang et al. (27) experimentally demonstrated that the H-Ras E31K mutant binds more tightly to the RalGDS RBD compared to the WT H-Ras. Our findings, together with the experimental confirmation, explain that the strength of Rap1–RBD indeed arises due to the presence of Lys31^{Rap1}. Moreover, our analysis revealed two important interactions in mutant systems: Glu37^{Ras}–Ser817^{RBD} and Glu37^{Ras}–Tyr815^{RBD} interactions

Please cite this article in press as: Demirbas et al., G12 mutations rewire allosteric communication at the Ras–RalGDS interface, Biophysical Journal (2026), https://doi.org/10.1016/j.bpj.2026.01.053

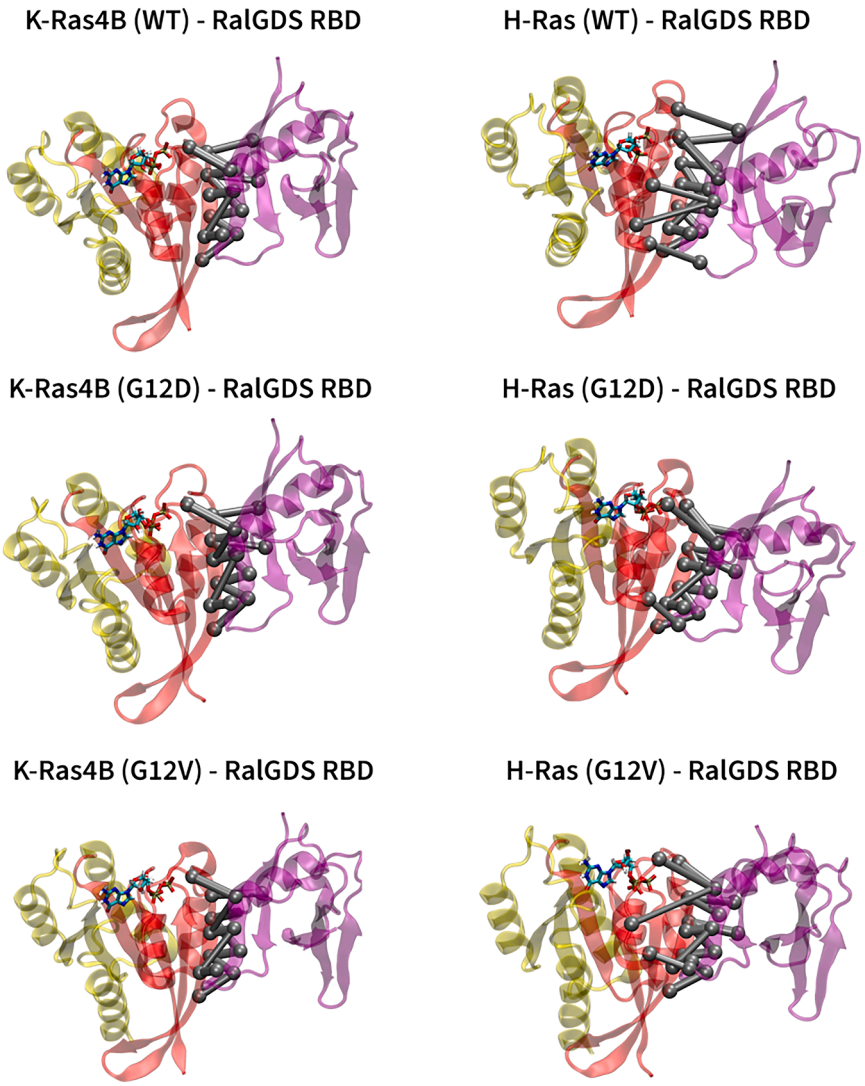


FIGURE 7 Interface networks for the K-Ras4B and H-Ras systems. The column on the left represents the K-Ras4B complexes, and the column on the right represents the H-Ras complexes. The interface edges and nodes are in gray. Catalytic Ras domain (residues 1–86) is in red, allosteric Ras domain (residues 87–167) is in yellow, and RalGDS is in purple. Edges with a frequency of 33% or higher are shown.

were amplified in both isoforms upon G12 mutations. This modification was accompanied by a loss in the $Asp38^{Ras}$–$Ser817^{RBD}$ interaction, suggesting that G12 mutations favor Glu37-mediated stabilization in switch I. Also, we observed that K-Ras4B mutants prefer the $Asp38^{Ras}$–$Lys836^{RBD}$ salt bridge over $Asp38^{Ras}$–$Lys816^{RBD}$.

Importantly, the $Asp38^{Ras}$–$Lys836^{RBD}$ salt bridge corresponds to the unique interface edge identified in the interface communication networks of K-Ras4B mutant systems, indicating that it not only stabilizes the interface but also transduces allosteric signals across the complex. Also, communication between $Asp38^{Ras}$–$Ser817^{RBD}$ was only seen in WT systems, consistent with bonding profiles. This observation suggests a direct mechanistic coupling between local electrostatic stabilization in the interface and long-range allosteric communication. It appears that G12 mutations reshape the energetic landscape of the interface, modifying routes for signal propagation by (dis)favoring specific electrostatic interactions. We had similarly observed that allosteric pathways differ between the open and closed conformations of K-Ras4B in a partner-specific way for GDP- and GNP-bound forms (67).

Binding free energy results showed that all simulated complexes were energetically favorable. Among the WT systems, Rap1–RBD interaction is the strongest, with a binding free energy of -55.6 ± 2.2 kcal/mol, and this highest strength might explain the regulatory antagonist effect of Rap1 on RalGDS. In contrast, M-Ras–RBD interaction is the weakest with a binding free energy of -36.0 ± 2.4 kcal/mol. The binding free energy values are similar for the K-Ras4B and H-Ras systems within the error range, regardless of isoform or mutation. It should be noted that MM/GBSA, as an end-state, implicit-solvent approximation, fails to reproduce absolute binding free energy values measured experimentally, with reported deviations ranging from 20 kcal/mol to 120 kcal/mol (68). These deviations

Please cite this article in press as: Demirbas et al., G12 mutations rewire allosteric communication at the Ras–RalGDS interface, Biophysical Journal (2026), https://doi.org/10.1016/j.bpj.2026.01.053

TABLE 1 Interface connections between Ras and RalGDS RBD

System	Interface connections	Interface nodes	Interface Ras nodes	Interface RalGDS nodes
H-Ras^{WT}	13 ± 1.0	19 ± 1.5	9.7 ± 0.9	9.3 ± 0.7
H-Ras^{G12D}	12.6 ± 1.3	17 ± 1.5	8.7 ± 0.9	8.3 ± 0.7
H-Ras^{G12V}	10.3 ± 2.7	15 ± 3.6	7.7 ± 1.9	7.3 ± 1.8
K-Ras4B^{WT}	11.3 ± 1.2	16 ± 0.6	7.7 ± 0.3	8.3 ± 0.3
K-Ras4B^{G12D}	11.3 ± 0.3	14.7 ± 0.6	7.0 ± 0.0	7.6 ± 0.3
K-Ras4B^{G12V}	12.7 ± 1.7	17.6 ± 2.0	8.7 ± 0.9	9.0 ± 1.2

are mainly caused by the treatment of solvation using implicit solvent models and by unaccounted-for conformational fluctuations between the free and bound proteins (69). Nevertheless, MM/GBSA is known to be more successful at ranking structurally similar complexes (69), which is our aim in this study. Therefore, given its low computational cost, we preferred it to alchemical methods such as free energy perturbation or thermodynamic integration, which are known to better reproduce experimental results (70). Thus, the results should be regarded as qualitative trends rather than precise quantitative rankings among closely related Ras systems. Since MM/GBSA calculations primarily account for interfacial interactions, slight changes in bonding profiles can affect the calculated energy, as evidenced by the relatively large standard deviation observed for H-Ras^{G12V}.

It is known that oncogenic Ras mutations do not always increase Ras binding affinity for downstream effectors (71). Many of them increase signaling primarily by shifting the GTP-bound Ras ensemble to the active state, which in turn increases the population of effector-bound complexes even when intrinsic affinity is not higher (72). Therefore, we further analyzed the allosteric communication pathways to uncover how G12 mutations affect complex dynamics. Both WT complexes reveal a coupling between Gly12^{Ras} and GTP that reflects the well-recognized role of Gly12^{Ras} in catalysis. This link is not as persistent in the mutant systems, where the links between Asp/Val12^{Ras}–Gln61^{Ras}, Tyr64^{Ras}–Ile36^{Ras}, and Ile36^{Ras}–Ile803^{RBD} are generally amplified compared to the WTs. It is known that G12 mutations render the catalytic activity of Gln61^{Ras} by disturbing its side chain (72). Therefore, we propose that this rewiring disrupts the catalytic activity while biasing the Ras conformation toward effector-competent states. The allosteric route Gln61^{Ras}–Tyr64^{Ras}–Ile36^{Ras}–Ile803^{RBD} was observed in all complexes. This observation is in line with previous studies that have demonstrated impaired RalGDS activity upon mutations seen at Ile36^{Ras} and Tyr64^{Ras} (35,73).

H-Ras and K-Ras4B have 100% identical effector lobe and 90% identical allosteric lobe sequences. It is known that the diverse biochemical properties of Ras proteins are regulated mainly by their hypervariable regions (HVRs), which interact with the plasma membrane and ultimately determine membrane distributions of Ras isoforms (74,75). However, the HVR does not directly participate in effector binding, and previous studies suggest that oncogenic mutations, including G12D/V, decouple the catalytic domain and HVR, as evidenced by the reduced interaction energy between the two regions upon mutation (76). The slightly increased RMSF values for the residues around the C-terminus for some systems may be attributed to the absence of C-terminal restraints present in membrane-anchored Ras. Nonetheless, although only G-domains were simulated in this study, excluding HVRs, we were able to capture differences between K-Ras4B–RBD and H-Ras–RBD interactions as well as the effects of G12D/V mutations. This proves that the G-domain alone is sufficient to make some deductions about the differential behaviors of H-Ras and K-Ras4B in their interaction with the RalGDS RBD.

TABLE 2 Number of edges and nodes in each system's metapath

System	Metapath nodes	Metapath edges	Metapath Ras nodes	Metapath RalGDS nodes
H-Ras^{WT}	72.3 ± 7.3	73.6 ± 10.6	47.6 ± 5.2	25.7 ± 4.7
H-Ras^{G12D}	53.6 ± 8.1	55.5 ± 8.4	30 ± 4.3	23 ± 4.5
H-Ras^{G12V}	72.3 ± 7.2	81.3 ± 7.1	53.3 ± 6.5	24 ± 4.3
K-Ras4B^{WT}	60.3 ± 10.5	60.6 ± 10.2	33.6 ± 6.3	23.3 ± 1.8
K-Ras4B^{G12D}	70.6 ± 1.8	74.3 ± 3.2	45 ± 3.5	24.6 ± 3.5
K-Ras4B^{G12V}	74 ± 4.0	80.6 ± 4.1	49.6 ± 0.3	25.6 ± 1.5

CONCLUSION

Despite numerous studies indicating the importance of the Ras/RalGDS/Ral pathway in human oncogenesis, the atomistic-level details of the interaction between Ras family members/mutants and the RalGDS RBD have been underinvestigated. By conducting long-timescale MD simulations of different Ras family members and their mutants in complex with GTP, we aimed to fill this void in the literature. Interaction profiles, critical residues, differential dynamics of the switch I and switch II regions, and some allosteric regulations in the Ras–RBD interaction were identified and discussed in detail. Isoform- and mutant-specific critical residues and interactions were detected. As mentioned in the earlier sections, Ral overactivity is a hallmark of aggressive metastatic behavior in Ras$^{G12D/V}$-driven pancreatic cancer and colorectal cancers. Proposed interaction dynamics for the mutant systems may serve as a good reference point for studies aiming to develop mutant-specific targeting strategies against Ras-driven tumors.

DATA AND CODE AVAILABILITY

The data that support the findings of this study are available from the corresponding authors upon reasonable request.

Please cite this article in press as: Demirbas et al., G12 mutations rewire allosteric communication at the Ras–RalGDS interface, Biophysical Journal (2026), https://doi.org/10.1016/j.bpj.2026.01.053

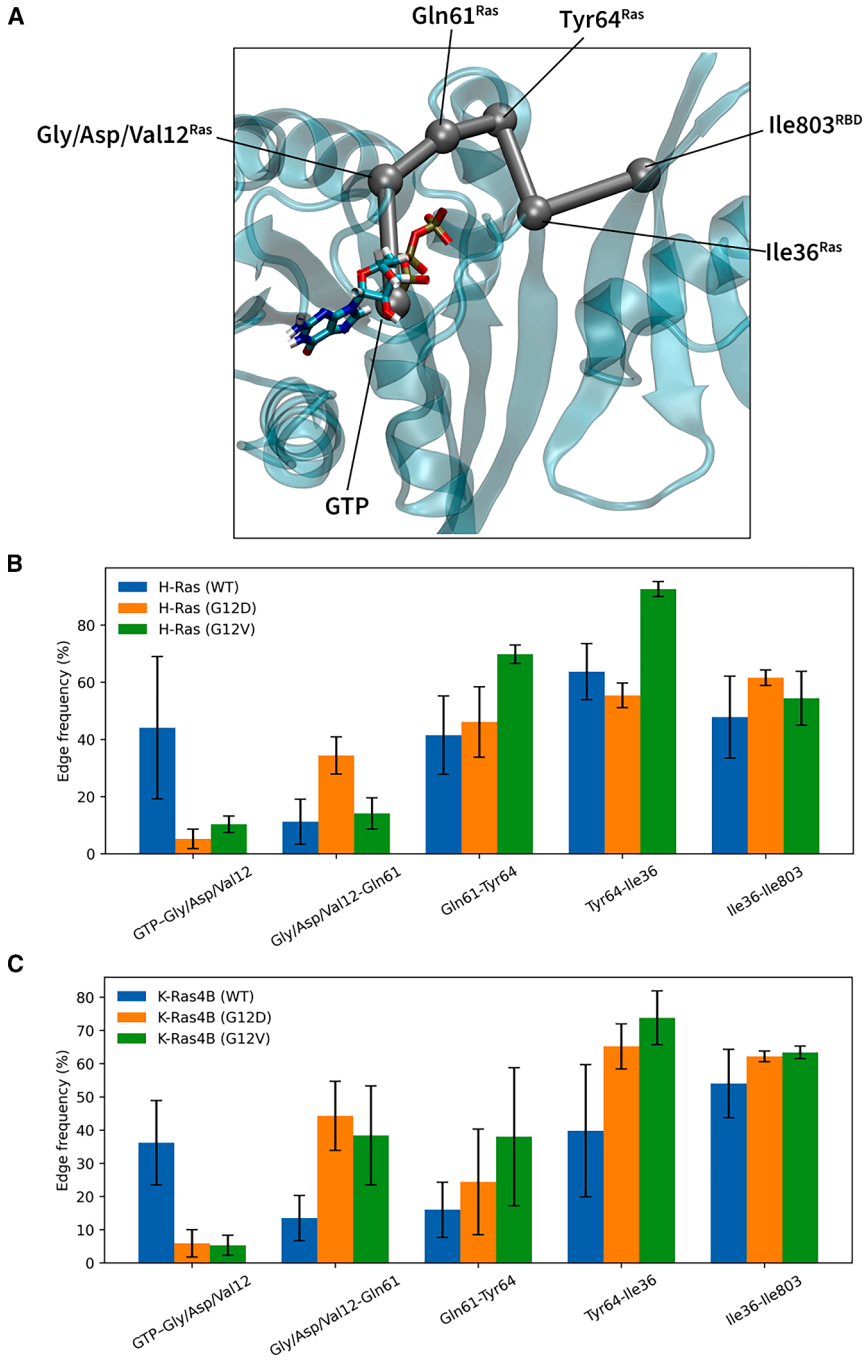


FIGURE 8 Allosteric communication analysis. (*A*) The allosteric route GTP–Gly/Asp/Val12^{Ras}–Gln61^{Ras}–Tyr64^{Ras}–Ile36^{Ras}–Ile803^{RBD}. The edges and nodes are in gray. (*B*) Edge frequencies of H-Ras systems. Blue, orange, and green bars represent H-Ras^{WT}, H-Ras^{G12D}, and H-Ras^{G12V}, respectively. (*C*) Edge frequencies of K-Ras4B systems. Blue, orange, and green bars represent K-Ras4B^{WT}, K-Ras4B^{G12D}, and K-Ras4B^{G12V}, respectively. Data are presented as mean ± SEM.

ACKNOWLEDGMENTS

This research was supported by the Cancer Innovation Laboratory, Center for Cancer Research, National Cancer Institute, National Institutes of Health (NIH) Intramural Research Program project number ZIA BC 010441, and federal funds from the National Cancer Institute, NIH under contract HHSN261201500003I. The contributions of the NIH authors were made as part of their official duties as NIH federal employees, are in compliance with agency policy requirements, and are considered Works of the United States Government. However, the findings and conclusions presented in this paper are those of the authors and do not necessarily reflect the views of the NIH or the US Department of Health and Human Services. Simulations were performed using the high-performance computational facilities of the Biowulf PC/Linux cluster at the NIH, Bethesda, MD (https://hpc.nih.gov/) and the KUACC HPC at Koc University, Istanbul.

AUTHOR CONTRIBUTIONS

R.N., H.J., O.K., and A.G. conceived the project; E.D., K.K., and H.J. performed the simulations; E.D. analyzed the data; E.D. and K.K. wrote the first draft; R.N., H.J., O.K., and A.G. made critical revisions; and all authors

contributed to the interpretation of the results and approved the final manuscript.

DECLARATION OF INTERESTS

The authors declare no competing interests.

SUPPORTING MATERIAL

Supporting material can be found online at https://doi.org/10.1016/j.bpj.2026.01.053.

REFERENCES

1. Yin, G., J. Huang, …, Y. Gao. 2023. Targeting small GTPases: emerging grasps on previously untamable targets, pioneered by KRAS. *Signal Transduct. Target. Ther.* 8:212. https://doi.org/10.1038/s41392-023-01441-4.
2. Mozzarelli, A. M., D. K. Simanshu, and P. Castel. 2024. Functional and structural insights into RAS effector proteins. *Mol. Cell.* 84:2807–2821. https://doi.org/10.1016/j.molcel.2024.06.027.
3. Song, S., W. Cong, …, Q. Zhang. 2019. Small GTPases: Structure, biological function and its interaction with nanoparticles. *Asian J. Pharm. Sci.* 14:30–39. https://doi.org/10.1016/j.ajps.2018.06.004.
4. Lu, S., H. Jang, …, J. Zhang. 2016. Ras Conformational Ensembles, Allostery, and Signaling. *Chem. Rev.* 116:6607–6665. https://doi.org/10.1021/acs.chemrev.5b00542.
5. Catozzi, S., C. Ternet, …, C. Kiel. 2022. Reconstruction and analysis of a large-scale binary Ras-effector signaling network. *Cell Commun. Signal.* 20:24. https://doi.org/10.1186/s12964-022-00823-5.
6. Gasper, R., and F. Wittinghofer. 2019. The Ras switch in structural and historical perspective. *Biol. Chem.* 401:143–163. https://doi.org/10.1515/hsz-2019-0330.
7. Kolch, W., D. Berta, and E. Rosta. 2023. Dynamic regulation of RAS and RAS signaling. *Biochem. J.* 480:1–23. https://doi.org/10.1042/BCJ20220234.
8. Johnson, C. W., D. Reid, …, C. Mattos. 2017. The small GTPases K-Ras, N-Ras, and H-Ras have distinct biochemical properties determined by allosteric effects. *J. Biol. Chem.* 292:12981–12993. https://doi.org/10.1074/jbc.M117.778886.
9. Yang, X., and H. Wu. 2024. RAS signaling in carcinogenesis, cancer therapy and resistance mechanisms. *J. Hematol. Oncol.* 17:108. https://doi.org/10.1186/s13045-024-01631-9.
10. Burge, R. A., and G. A. Hobbs. 2022. Not all RAS mutations are equal: A detailed review of the functional diversity of RAS hot spot mutations. *Adv. Cancer Res.* 153:29–61. https://doi.org/10.1016/bs.acr.2021.07.004.
11. Xu, S., B. N. Long, …, M. A. Kennedy. 2017. Structural insight into the rearrangement of the switch I region in GTP-bound G12A K-Ras. *Acta Crystallogr. D Struct. Biol.* 73:970–984. https://doi.org/10.1107/S2059798317015418.
12. Fetics, S. K., H. Guterres, …, C. Mattos. 2015. Allosteric effects of the oncogenic RasQ61L mutant on Raf-RBD. *Structure.* 23:505–516. https://doi.org/10.1016/j.str.2014.12.017.
13. Yan, C., and D. Theodorescu. 2018. RAL GTPases: Biology and Potential as Therapeutic Targets in Cancer. *Pharmacol. Rev.* 70:1–11. https://doi.org/10.1124/pr.117.014415.
14. Chardin, P., and A. Tavitian. 1986. The ral gene: a new ras related gene isolated by the use of a synthetic probe. *EMBO J.* 5:2203–2208. https://doi.org/10.1002/j.1460-2075.1986.tb04485.x.
15. Ghoroghi, S., A. Larnicol, …, V. Hyenne. 2021. Ral GTPases promote breast cancer metastasis by controlling biogenesis and organ targeting of exosomes. *eLife.* 10:e61539. https://doi.org/10.7554/eLife.61539.
16. Nászai, M., K. B. Yachuan, …, J. B. Cordero. 2021. RAL GTPases mediate EGFR-driven intestinal stem cell proliferation and tumourigenesis. *eLife.* 10:e63807. https://doi.org/10.7554/eLife.63807.
17. Lim, K.-H., A. T. Baines, …, C. M. Counter. 2005. Activation of RalA is critical for Ras-induced tumorigenesis of human cells. *Cancer Cell.* 7:533–545. https://doi.org/10.1016/j.ccr.2005.04.030.
18. Tchevkina, E., L. Agapova, …, A. Tatosyan. 2005. The small G-protein RalA stimulates metastasis of transformed cells. *Oncogene.* 24:329–335. https://doi.org/10.1038/sj.onc.1208094.
19. Cao, M., X. Li, …, H. Horiuchi. 2023. Ral GTPase promotes metastasis of pancreatic ductal adenocarcinoma via elevation of TGF-β1 production. *J. Biol. Chem.* 299:104754. https://doi.org/10.1016/j.jbc.2023.104754.
20. Neel, N. F., K. L. Rossman, …, C. J. Der. 2012. The RalB Small GTPase Mediates Formation of Invadopodia through a GTPase-Activating Protein-Independent Function of the RalBP1/RLIP76 Effector. *Mol. Cell Biol.* 32:1374–1386. https://doi.org/10.1128/MCB.06291-11.
21. Neel, N. F., T. D. Martin, …, C. J. Der. 2011. The RalGEF-Ral Effector Signaling Network. *Genes Cancer.* 2:275–287. https://doi.org/10.1177/1947601911407329.
22. Gentry, L. R., T. D. Martin, …, C. J. Der. 2014. Ral small GTPase signaling and oncogenesis: More than just 15 minutes of fame. *Biochim. Biophys. Acta.* 1843:2976–2988. https://doi.org/10.1016/j.bbamcr.2014.09.004.
23. Ferro, E., and L. Trabalzini. 2010. RalGDS family members couple Ras to Ral signalling and that's not all. *Cell. Signal.* 22:1804–1810. https://doi.org/10.1016/j.cellsig.2010.05.010.
24. Yin, J., C. Pollock, …, K. Kelly. 2007. Activation of the RalGEF/Ral Pathway Promotes Prostate Cancer Metastasis to Bone. *Mol. Cell Biol.* 27:7538–7550. https://doi.org/10.1128/MCB.00955-07.
25. Johansson, J., M. Naszai, …, O. J. Sansom. 2019. RAL GTPases Drive Intestinal Stem Cell Function and Regeneration through Internalization of WNT Signalosomes. *Cell Stem Cell.* 24:592–607.e7. https://doi.org/10.1016/j.stem.2019.02.002.
26. González-García, A., C. A. Pritchard, …, C. J. Marshall. 2005. RalGDS is required for tumor formation in a model of skin carcinogenesis. *Cancer Cell.* 7:219–226. https://doi.org/10.1016/j.ccr.2005.01.029.
27. Huang, L., F. Hofer, …, S.-H. Kim. 1998. Structural basis for the interaction of Ras with RalGDS. *Nat. Struct. Biol.* 5:422–426. https://doi.org/10.1038/nsb0698-422.
28. Hofer, F., S. Fields, …, G. S. Martin. 1994. Activated Ras interacts with the Ral guanine nucleotide dissociation stimulator. *Proc. Natl. Acad. Sci. USA.* 91:11089–11093. https://doi.org/10.1073/pnas.91.23.11089.
29. Herrmann, C., G. Horn, …, A. Wittinghofer. 1996. Differential Interaction of the Ras Family GTP-binding Proteins H-Ras, Rap1A, and R-Ras with the Putative Effector Molecules Raf Kinase and Ral-Guanine Nucleotide Exchange Factor. *J. Biol. Chem.* 271:6794–6800. https://doi.org/10.1074/jbc.271.12.6794.
30. Spaargaren, M., and J. R. Bischoff. 1994. Identification of the guanine nucleotide dissociation stimulator for Ral as a putative effector molecule of R-ras, H-ras, K-ras, and Rap. *Proc. Natl. Acad. Sci. USA.* 91:12609–12613. https://doi.org/10.1073/pnas.91.26.12609.
31. Urano, T., R. Emkey, and L. A. Feig. 1996. Ral-GTPases mediate a distinct downstream signaling pathway from Ras that facilitates cellular transformation. *EMBO J.* 15:810–816.
32. Rodriguez-Viciana, P., C. Sabatier, and F. McCormick. 2004. Signaling Specificity by Ras Family GTPases Is Determined by the Full Spectrum of Effectors They Regulate. *Mol. Cell Biol.* 24:4943–4954. https://doi.org/10.1128/MCB.24.11.4943-4954.2004.
33. Young, L. C., and P. Rodriguez-Viciana. 2018. MRAS: A Close but Understudied Member of the RAS Family. *Cold Spring Harb. Perspect. Med.* 8:a033621. https://doi.org/10.1101/cshperspect.a033621.
34. Nussinov, R., H. Jang, …, A. A. Sablina. 2020. The Mystery of Rap1 Suppression of Oncogenic Ras. *Trends Cancer.* 6:369–379. https://doi.org/10.1016/j.trecan.2020.02.002.

Please cite this article in press as: Demirbas et al., G12 mutations rewire allosteric communication at the Ras–RalGDS interface, Biophysical Journal (2026), https://doi.org/10.1016/j.bpj.2026.01.053

35. Linnemann, T., C. Kiel, …, C. Herrmann. 2002. The Activation of RalGDS Can Be Achieved Independently of Its Ras Binding Domain. *J. Biol. Chem.* 277:7831–7837. https://doi.org/10.1074/jbc.m110800200.

36. Wohlgemuth, S., C. Kiel, …, C. Herrmann. 2005. Recognizing and Defining True Ras Binding Domains I: Biochemical Analysis. *J. Mol. Biol.* 348:741–758. https://doi.org/10.1016/j.jmb.2005.02.048.

37. Nakhaeizadeh, H., E. Amin, …, M. R. Ahmadian. 2016. The RAS-Effector Interface: Isoform-Specific Differences in the Effector Binding Regions. *PLoS One.* 11:e0167145. https://doi.org/10.1371/journal.pone.0167145.

38. Matsubara, K., S. Kishida, …, A. Kikuchi. 1999. Plasma membrane recruitment of RalGDS is critical for Ras-dependent Ral activation. *Oncogene.* 18:1303–1312. https://doi.org/10.1038/sj.onc.1202425.

39. Sayin, A. Z., Z. Abali, …, O. Keskin. 2024. Conformational diversity and protein–protein interfaces in drug repurposing in Ras signaling pathway. *Sci. Rep.* 14:1239. https://doi.org/10.1038/s41598-023-50913-8.

40. Baspinar, A., E. Cukuroglu, …, A. Gursoy. 2014. PRISM: a web server and repository for prediction of protein–protein interactions and modeling their 3D complexes. *Nucleic Acids Res.* 42:W285–W289. https://doi.org/10.1093/nar/gku397.

41. Yang, Z., K. Lasker, …, T. E. Ferrin. 2012. UCSF Chimera, MODELLER, and IMP: An integrated modeling system. *J. Struct. Biol.* 179:269–278. https://doi.org/10.1016/j.jsb.2011.09.006.

42. Best, R. B., X. Zhu, …, A. D. MacKerell, Jr. 2012. Optimization of the Additive CHARMM All-Atom Protein Force Field Targeting Improved Sampling of the Backbone ϕ, ψ and Side-Chain $\chi1$ and $\chi2$ Dihedral Angles. *J. Chem. Theory Comput.* 8:3257–3273. https://doi.org/10.1021/ct300400x.

43. Brooks, B. R., C. L. Brooks, III, …, M. Karplus. 2009. CHARMM: The Biomolecular Simulation Program. *J. Comput. Chem.* 30:1545–1614. https://doi.org/10.1002/jcc.21287.

44. Martyna, G. J., D. J. Tobias, and M. L. Klein. 1994. Constant pressure molecular dynamics algorithms. *J. Chem. Phys.* 101:4177–4189. https://doi.org/10.1063/1.467468.

45. Essmann, U., L. Perera, …, L. G. Pedersen. 1995. A smooth particle mesh Ewald method. *J. Chem. Phys.* 103:8577–8593. https://doi.org/10.1063/1.470117.

46. Phillips, J. C., R. Braun, …, K. Schulten. 2005. Scalable Molecular Dynamics with NAMD. *J. Comput. Chem.* 26:1781–1802. https://doi.org/10.1002/jcc.20289.

47. Kollman, P. A., I. Massova, …, T. E. Cheatham. 2000. Calculating Structures and Free Energies of Complex Molecules: Combining Molecular Mechanics and Continuum Models. *Acc. Chem. Res.* 33:889–897. https://doi.org/10.1021/ar000033j.

48. Schlitter, J. 1993. Estimation of absolute and relative entropies of macromolecules using the covariance matrix. *Chem. Phys. Lett.* 215:617–621. https://doi.org/10.1016/0009-2614(93)89366-P.

49. Andricioaei, I., and M. Karplus. 2001. On the calculation of entropy from covariance matrices of the atomic fluctuations. *J. Chem. Phys.* 115:6289–6292. https://doi.org/10.1063/1.1401821.

50. Case, D. A., H. M. Aktulga, …, M. Merz. 2023. AmberTools. *J. Chem. Inf. Model.* 63:6183–6191. https://doi.org/10.1021/acs.jcim.3c01153.

51. Miller, B. R., III, T. D. McGee, Jr, …, A. E. Roitberg. 2012. MMPBSA.py: An Efficient Program for End-State Free Energy Calculations. *J. Chem. Theory Comput.* 8:3314–3321. https://doi.org/10.1021/ct300418.

52. Shirts, M. R., C. Klein, …, E. D. Zhong. 2017. Lessons learned from comparing molecular dynamics engines on the SAMPL5 dataset. *J. Comput. Aided Mol. Des.* 31:147–161. https://doi.org/10.1007/s10822-016-9977-1.

53. Onufriev, A., D. Bashford, and D. A. Case. 2004. Exploring protein native states and large-scale conformational changes with a modified generalized born model. *Proteins.* 55:383–394. https://doi.org/10.1002/prot.20033.

54. McGibbon, R. T., K. A. Beauchamp, …, V. S. Pande. 2015. MDTraj: A Modern Open Library for the Analysis of Molecular Dynamics Trajectories. *Biophys. J.* 109:1528–1532. https://doi.org/10.1016/j.bpj.2015.08.015.

55. Humphrey, W., A. Dalke, and K. Schulten. 1996. VMD: Visual molecular dynamics. *J. Mol. Graph.* 14:33–38. https://doi.org/10.1016/0263-7855(96)00018-5.

56. Bosshard, H. R., D. N. Marti, and I. Jelesarov. 2004. Protein stabilization by salt bridges: concepts, experimental approaches and clarification of some misunderstandings. *J. Mol. Recognit.* 17:1–16. https://doi.org/10.1002/jmr.657.

57. Donald, J. E., D. W. Kulp, and W. F. DeGrado. 2011. Salt bridges: geometrically specific, designable interactions. *Proteins.* 79:898–915. https://doi.org/10.1002/prot.22927.

58. Felline, A., M. Seeber, and F. Fanelli. 2022. PSNtools for standalone and web-based structure network analyses of conformational ensembles. *Comput. Struct. Biotechnol. J.* 20:640–649. https://doi.org/10.1016/j.csbj.2021.12.044.

59. Gorfe, A. A., B. J. Grant, and J. A. McCammon. 2008. Mapping the nucleotide and isoform dependent structural and dynamical features of Ras proteins. *Structure.* 16:885–896. https://doi.org/10.1016/j.str.2008.03.009.

60. Kapoor, A., and A. Travesset. 2015. Differential dynamics of RAS isoforms in GDP- and GTP-bound states. *Proteins.* 83:1091–1106. https://doi.org/10.1002/prot.24805.

61. Lukman, S., B. J. Grant, …, J. A. McCammon. 2010. The Distinct Conformational Dynamics of K-Ras and H-Ras A59G. *PLoS Comput. Biol.* 6:e1000922. https://doi.org/10.1371/journal.pcbi.1000922.

62. Muratcioglu, S., C. Aydin, …, O. Keskin. 2020. Oncogenic K-Ras4B Dimerization Enhances Downstream Mitogen-activated Protein Kinase Signaling. *J. Mol. Biol.* 432:1199–1215. https://doi.org/10.1016/j.jmb.2020.01.002.

63. Chakrabarti, M., H. Jang, and R. Nussinov. 2016. Comparison of the Conformations of KRAS Isoforms, K-Ras4A and K-Ras4B, Points to Similarities and Significant Differences. *J. Phys. Chem. B.* 120:667–679. https://doi.org/10.1021/acs.jpcb.5b11110.

64. Lawson, A. R. J., F. Abascal, …, I. Martincorena. 2025. Somatic mutation and selection at population scale. *Nature.* 647:411–420. https://doi.org/10.1038/s41586-025-09584-w.

65. Vetter, I. R., T. Linnemann, …, A. Wittinghofer. 1999. Structural and biochemical analysis of Ras-effector signaling via RalGDS. *FEBS Lett.* 451:175–180. https://doi.org/10.1016/s0014-5793(99)00555-4.

66. Shirouzu, M., K. Hashimoto, …, S. Yokoyama. 1999. Double-Mutant Analysis of the Interaction of Ras with the Ras-Binding Domain of RGL. *Biochemistry.* 38:5103–5110. https://doi.org/10.1021/bi9820053.

67. Eren, M., N. Tuncbag, …, O. Keskin. 2021. Normal Mode Analysis of KRas4B Reveals Partner Specific Dynamics. *J. Phys. Chem. B.* 125:5210–5221. https://doi.org/10.1021/acs.jpcb.1c00891.

68. Sun, H., Y. Li, …, T. Hou. 2014. Assessing the performance of MM/PBSA and MM/GBSA methods. 4. Accuracies of MM/PBSA and MM/GBSA methodologies evaluated by various simulation protocols using PDBbind data set. *Phys. Chem. Chem. Phys.* 16:16719–16729. https://doi.org/10.1039/c4cp01388c.

69. Wang, E., H. Sun, …, T. Hou. 2019. End-Point Binding Free Energy Calculation with MM/PBSA and MM/GBSA: Strategies and Applications in Drug Design. *Chem. Rev.* 119:9478–9508. https://doi.org/10.1021/acs.chemrev.9b00055.

70. Adediwura, V. A., K. Koirala, …, Y. Miao. 2024. Understanding the impact of binding free energy and kinetics calculations in modern drug discovery. *Expert Opin. Drug Discov.* 19:671–682. https://doi.org/10.1080/17460441.2024.2349149.

71. Munoz-Maldonado, C., Y. Zimmer, and M. Medova. 2019. A Comparative Analysis of Individual RAS Mutations in Cancer Biology. *Front. Oncol.* 9:1088. https://doi.org/10.3389/fonc.2019.01088.

72. Lu, S., H. Jang, …, J. Zhang. 2016. The Structural Basis of Oncogenic Mutations G12, G13 and Q61 in Small GTPase K-Ras4B. *Sci. Rep.* 6:21949. https://doi.org/10.1038/srep21949.

Please cite this article in press as: Demirbas et al., G12 mutations rewire allosteric communication at the Ras–RalGDS interface, Biophysical Journal (2026), https://doi.org/10.1016/j.bpj.2026.01.053

73. Weng, C., A. J. Faure, …, B. Lehner. 2024. The energetic and allosteric landscape for KRAS inhibition. *Nature*. 626:643–652. https://doi.org/10.1038/s41586-023-06954-0.

74. Simanshu, D. K., D. V. Nissley, and F. McCormick. 2017. RAS Proteins and Their Regulators in Human Disease. *Cell*. 170:17–33. https://doi.org/10.1016/j.cell.2017.06.009.

75. Sayyed-Ahmad, A., P. Prakash, and A. A. Gorfe. 2017. Distinct dynamics and interaction patterns in H- and K-Ras oncogenic P-loop mutants. *Proteins*. 85:1618–1632. https://doi.org/10.1002/prot.25317.

76. Lu, S., A. Banerjee, …, R. Nussinov. 2015. GTP Binding and Oncogenic Mutations May Attenuate Hypervariable Region (HVR)-Catalytic Domain Interactions in Small GTPase K-Ras4B, Exposing the Effector Binding Site. *J. Biol. Chem.* 290:28887–28900. https://doi.org/10.1074/jbc.M115.664755.